Appendix B

Chapter 3

B-I Supplementary to 'Topological entanglement entropy to identify topological order in quantum skyrmions'

B-II Supplementary methods

To estimate the eigenstates, we used an exact diagonalisation method based on the **Lanczos** algorithm implemented on the open-source Python package QuSpin. This package employs a compressed row storage (CRS) sparse matrix format to handle the Hamiltonian and vectors, increasing the memory efficiency of the algorithm. Configuration of the CPU used was **Intel Xeon SKL G-6148** with 192 GB, DDR4 2666 MHz memory.

B-III Detailed Discussion on degeneracy

In fig. B.1 we have plotted degeneracy, Γ vs magnetic field, B for $J_2 = 0.2|J_1|$, $D = 2.0|J_1|$. The plot shows that the helical phase mainly has a six-fold degeneracy. When the system reaches the skyrmion phase from the helical phase, the degeneracy is lifted completely. Γ

remains nondegenerate in the skyrmion phase. We see that the plot shows exotic degenerate levels near the critical points of phase transition.

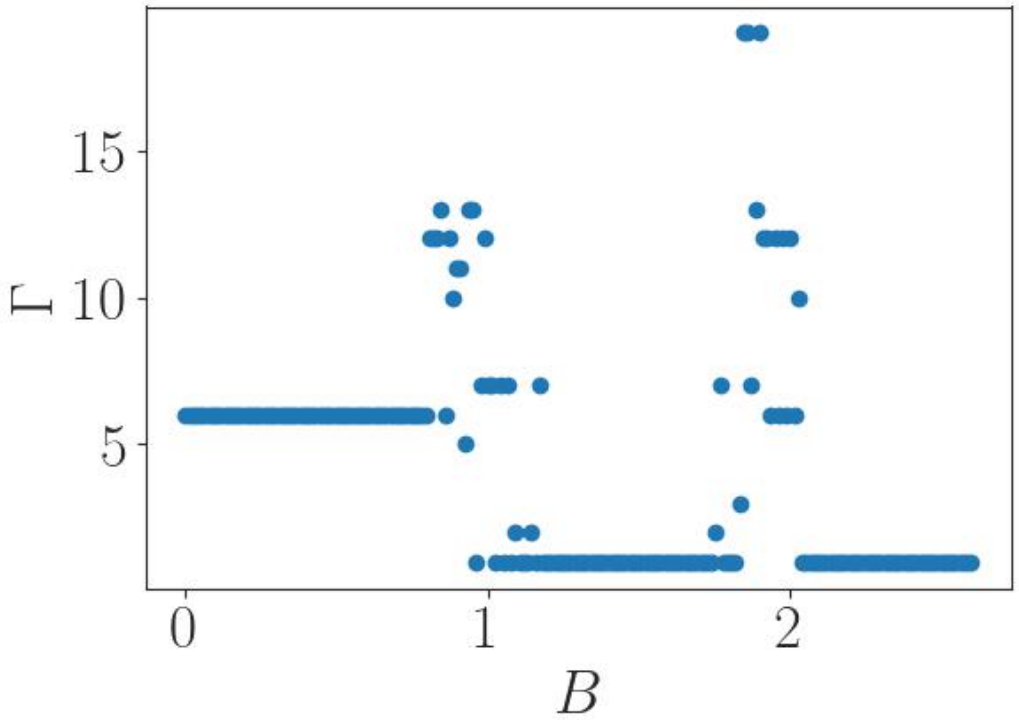

Fig. B.1 The degeneracy of the ground state, Γ is plotted against the applied field. We see that at low B values, GS has a degeneracy of $\Gamma = 6$. At very high B values, the degeneracy breaks and $\Gamma = 1$. Here for instance we considered $J_1 = -1.0$, $J_2 = 0.2|J_1|$, $D = 2.0|J_1|$.

Figure B.2 also indicates the degenerate states, explicitly plotting the energy levels vs B. Two such instances are shown. With larger J_2, the system requires large deformation to break the degeneracy.

$G_{\|}(\mathbf{q})$ is plotted for degenerate helical state in fig. B.3. We see that each degenerate state contributes differently to the noncolinear spin texture. Since the skyrmion and ferromagnetic phases are nondegenerate, we do not require such an illustration for those cases.

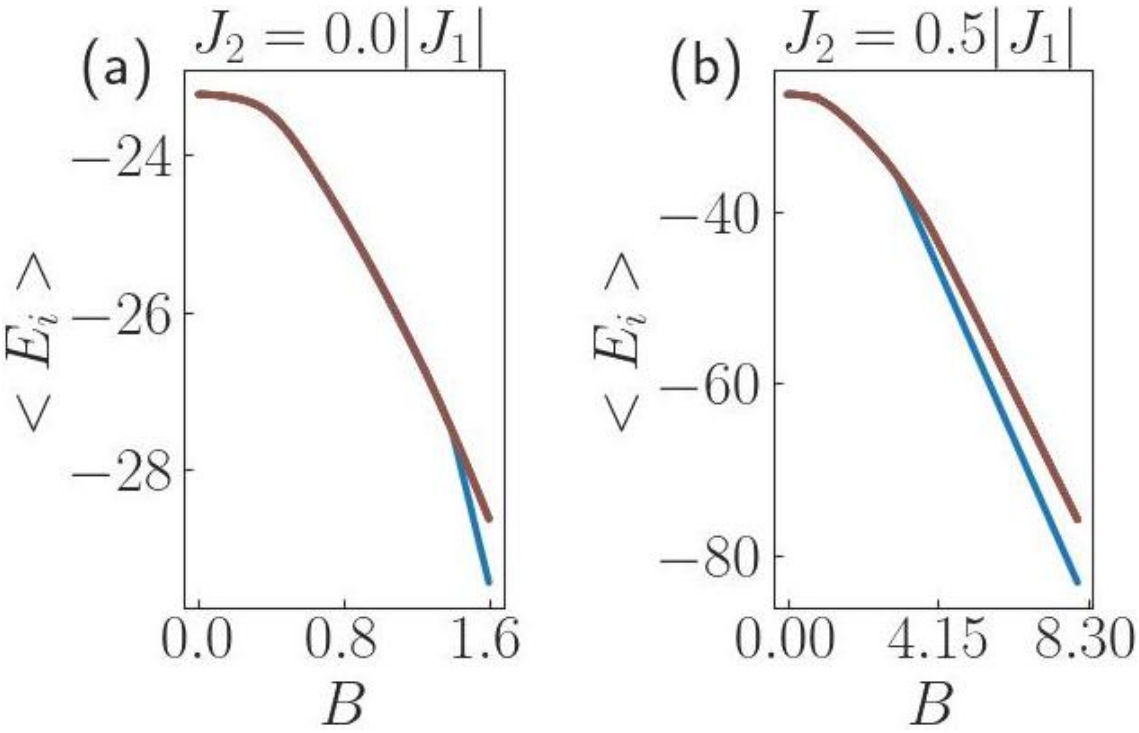

Fig. B.2 First six eigen energies plotted against the parameter B for (a) $J_2 = 0.0|J_1|$, $D = 2.0|J_1|$ and (b) $J_2 = 0.5|J_1|$, $D = 2.0|J_1|$. We see that they are degenerate up to a certain limit in B. The degeneracy breaks after a limit when B is increased in both cases.

We calculated the C_ψ for the first six energy eigenvectors and plotted them together in fig. B.4. Those curves are fairly smooth. But here, when we look at individual C_ψ for individual states, there appear to be significant fluctuations. Averaging helped to eliminate the fluctuations.

But in the case of $\mathscr{S}_{topo}$, the averaging did not remove the fluctuations, as we can see from fig. B.5. We did multiple random initialisations of the numeric calculation; all produced the same result. From this graph, we presume that the fluctuation is not due to the artefact of numerical methods or finite-size effects.

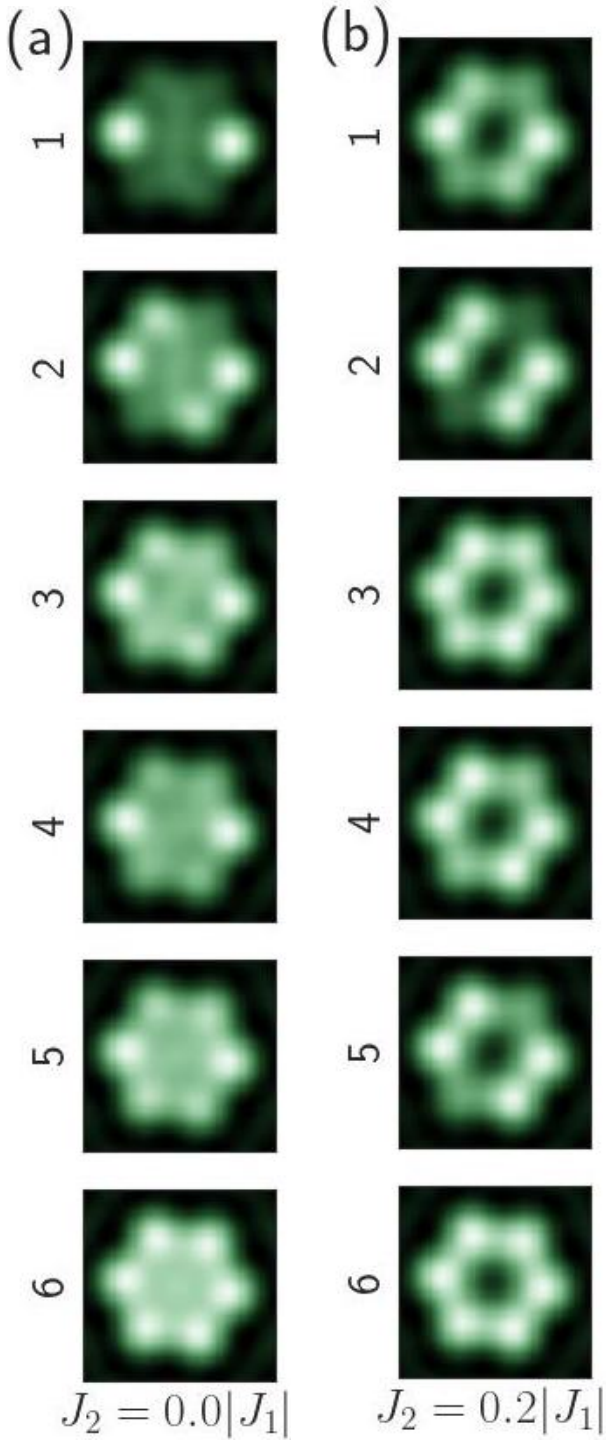

Fig. B.3 $G_{\parallel}(\mathbf{q})$ is calculated for each of the 6 degenerate ground state; (a) $J_2 = 0.0|J_1|$, $B = 0.4|J_1|$, $D = 2.0|J_1|$ and (b) $J_2 = 0.2|J_1|$, $B = 0.4|J_1|$, $D = 2.0|J_1|$. The non-collinearity of spins exists in all these states, as indicated by bright spots. Both (a) and (b) are instances where the system shows a six-fold degeneracy and is in the helical phase.

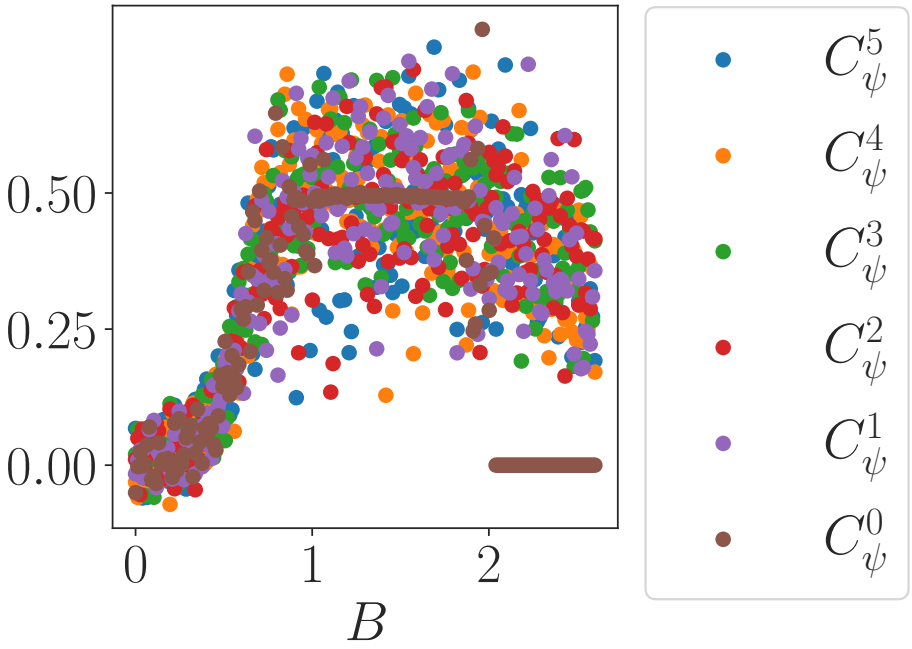

Fig. B.4 C_ψ for first six energy eigen vectors vs B for $J_2 = 0.2|J_1|$, $D = 2.0|J_1|$.

B-IV $\mathscr{S}_{\text{topo}}$ boundary

Here, we have provided zoom-in to the plots of $\mathscr{S}_{topo}$ for easy observation of the critical points. In fig. B.6, we can see linear and fluctuating parts of $\mathscr{S}_{topo}$ partitioned by vertical dashed lines. This plot, along with C_ψ, can then be used to mark the phase transition between helical and skyrmion phases.

B-V Relation between the correlation length and parameter J_2

Okubo *et al.* [B154] reported experimental and numerical results where strong further nearest neighbour interaction results in an incommensurate spiral structure, and they are stabilised under a magnetic field to produce skyrmion lattice. We identified similar properties in the theoretical model we investigated as well and attribute this to the system mimicking bulk when J_2 is large. In fig. B.7 we have plotted correlation function $G(r_{ji})$ v/s

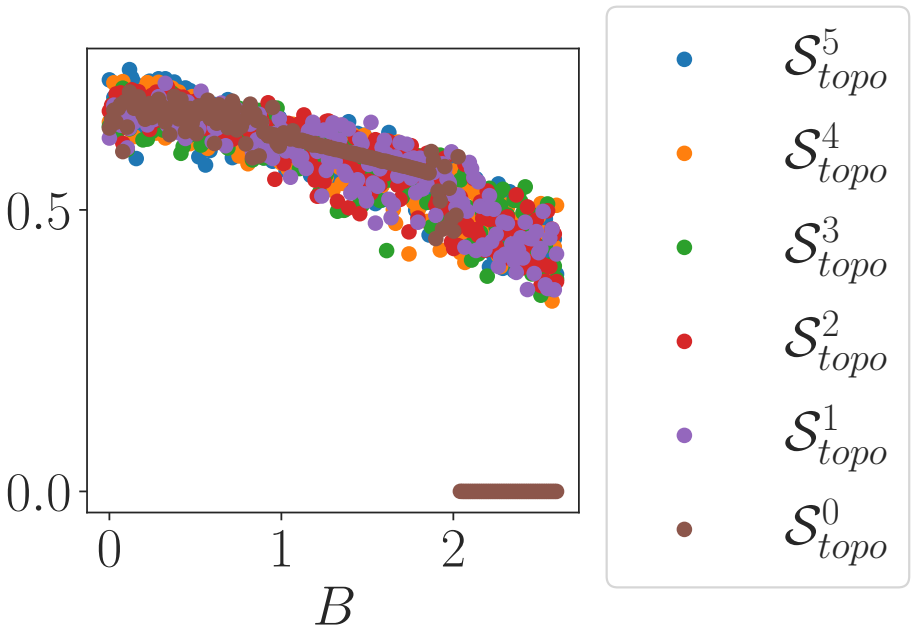

Fig. B.5 $\mathscr{S}_{topo}$ for first six energy eigen vectors plotted against B for $J_2 = 0.2|J_1|$, $D = 2.0|J_1|$.

r_{ji} for different skyrmions formed by parameters (J_2, B) in units of $|J_1|$. For larger J_2, the correlation function decays faster, implying a smaller correlation length. The results show that the correlation length decreases with increasing J_2. This indicates a lower correlation length for higher J_2. Compared to the system boundary, a shorter correlation length helps us comply with the condition Kitaev and Preskill consider for their definition of S_{topo}.

B-VI Fidelity

The fidelity of states corresponds to different B for $J_2 = 0.2|J_1|$, $D = 2.0|J_1|$ is shown in fig. B.8. Non-zero values mostly lie along the off-diagonal, indicating the orthogonality of states in different phases.

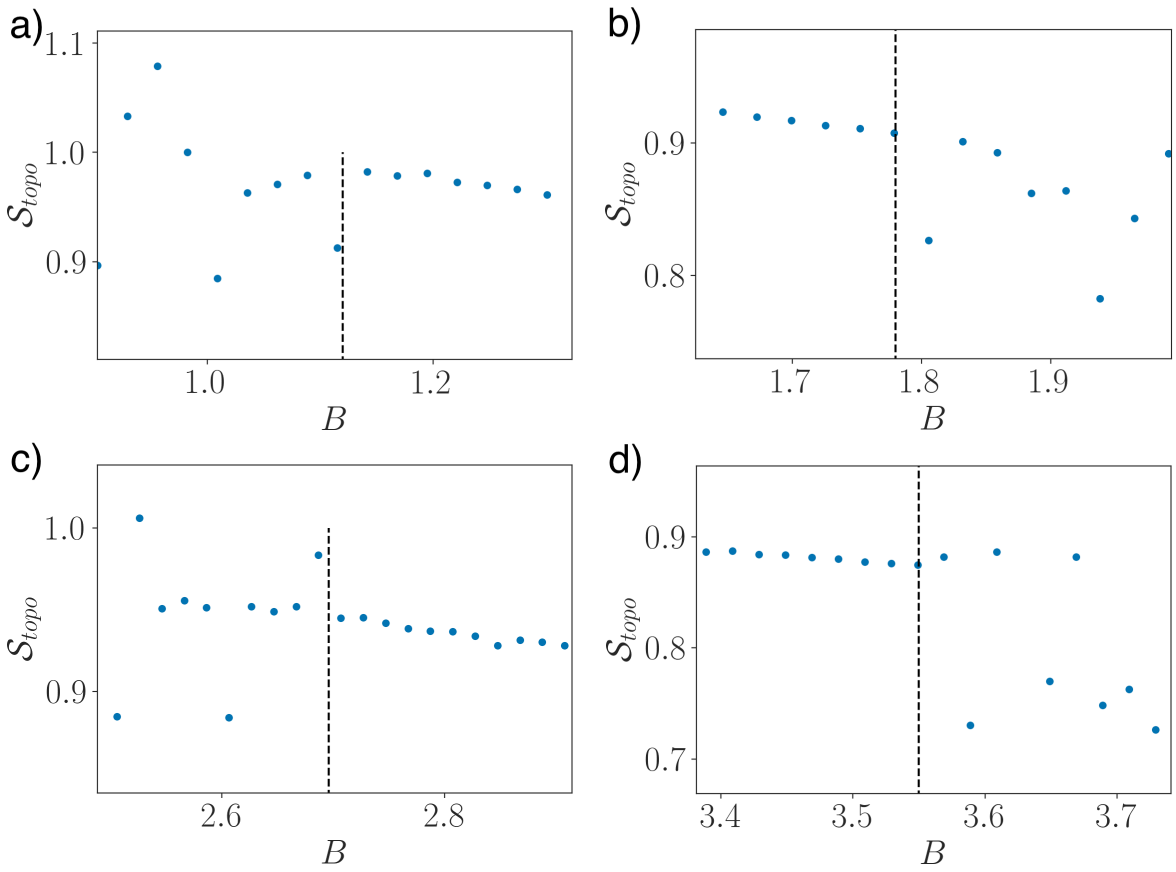

Fig. B.6 (a-b) shows the left (a) and right (b) boundary separating linear part and fluctuating parts of TEE for $J_2 = 0.2|J_1|$, $D = 2.0|J_1|$. (c-d) shows the same for $J_2 = 0.8|J_1|$, $D = 2.0|J_1|$.

B-VII Universality of fluctuating $\mathscr{S}_{\mathbf{topo}}$ in helical phase

We consider that the Hamiltonian of the spin-$\frac{1}{2}$ system has the form:

$$\hat{H} = B\sum_i \hat{S}_i^z + J_1 \sum_{\langle i,j\rangle} \hat{\vec{S}}_i\hat{\vec{S}}_j + \quad J_2 \sum_{\langle\langle i,j\rangle\rangle} \hat{\vec{S}}_i\hat{\vec{S}}_j + \sum_{ij} \mathbf{D}_{i,j}\left[\hat{\vec{S}}_i \times \hat{\vec{S}}_j\right], \tag{B.1}$$

Here, competing J_1 (ferromagnetic nearest-neighbour exchange) and J_2 (antiferromagnetic next-nearest neighbour exchange) interactions along with the Dzyaloshinskii-Moriya interaction (DMI) aid the formation of non-collinear magnetic textures. Single angle

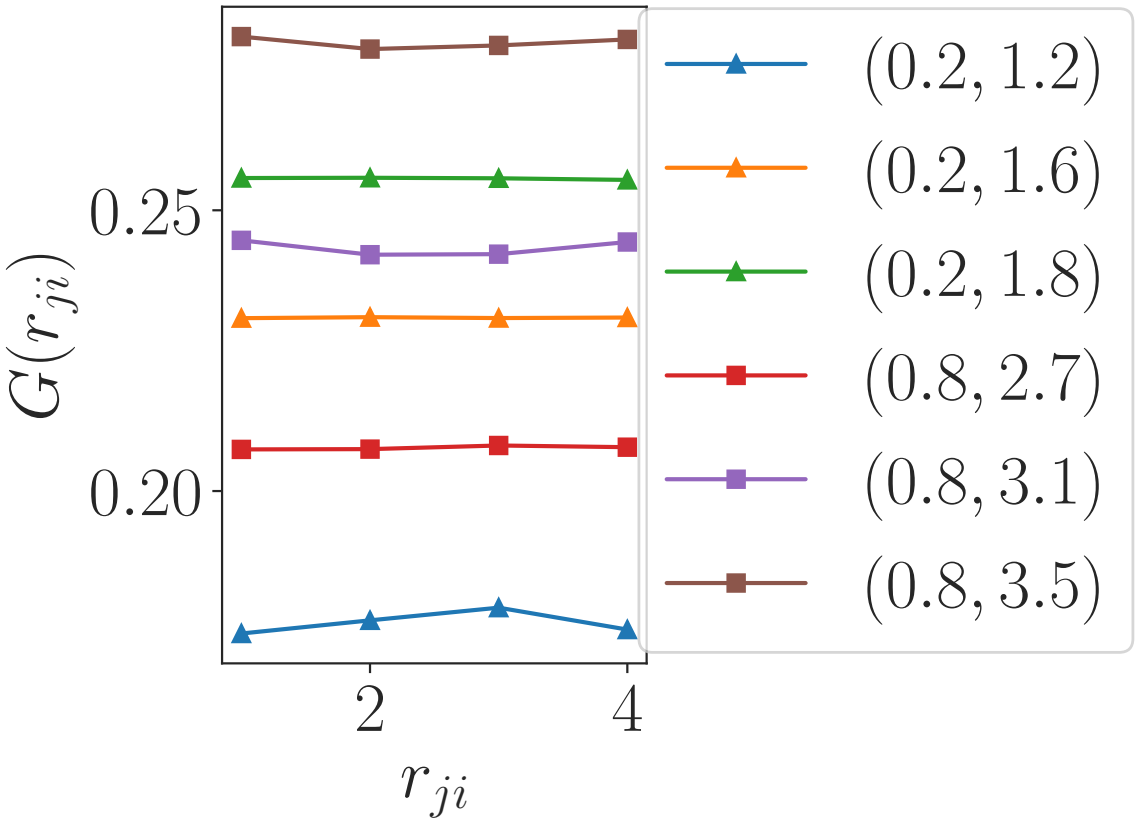

Fig. B.7 The correlation function $G_{||}(r_{ji})$ v/s r_{ji} between sites i and j. The legend (J_2, B) represents the respective parameters in $|J_1|$ units.

brackets denote summation over unique pairs of nearest neighbours, and double angle brackets denote summation over unique next-nearest neighbouring pairs. B is an external magnetic field, and the DM vector $\mathbf{D_{i,j}}$ is aligned perpendicular to the bond between lattice sites i and j . *i.e,* $\mathbf{D}_{i,j} = D\hat{e}_z \times (\mathbf{r}_j - \mathbf{r}_i)$ where $D = |\mathbf{D_{i,j}}|$. We verified the universality of the fluctuating TEE in the helical phase by studying TEE in different system sizes of the same Hamiltonian eq. B.1. The results are shown in fig. B.9. The fluctuation does not vanish/decrease with the increasing system size, implying that the fluctuation is not an artefact of finite size but is universal. The schematics for the spin lattices with $N = 7$ and $N = 13$ are provided in fig. B.10.

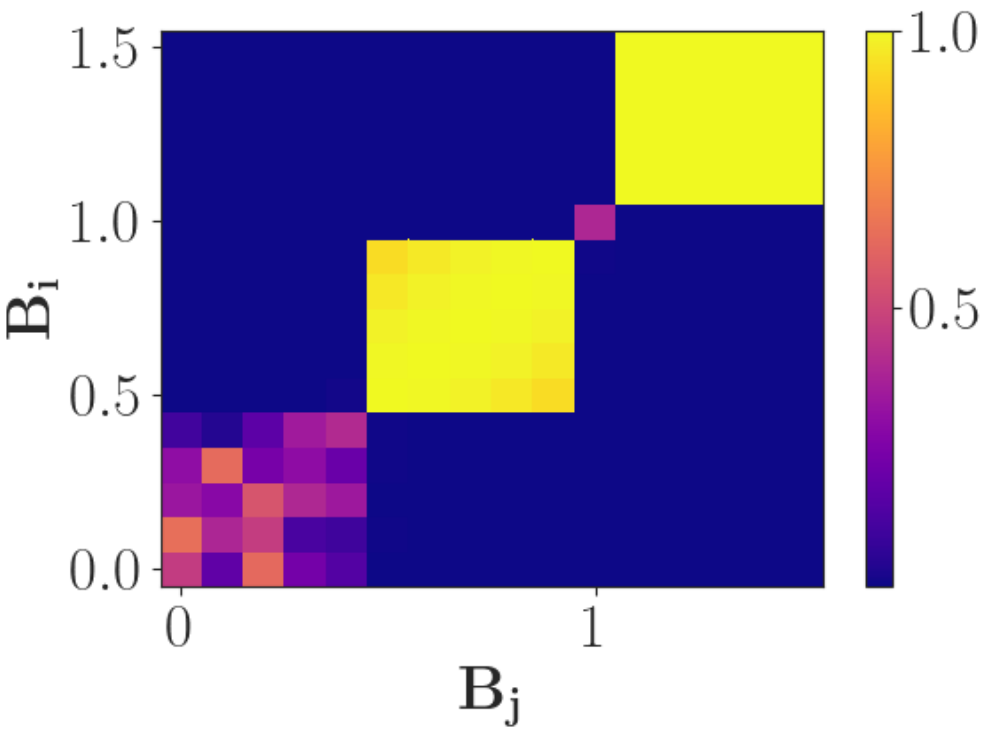

Fig. B.8 For $J_2 = 0.2|J_1|$ and $D = 2.0|J_1|$ fidelity of states $\langle\psi_i|$ and $|\psi_j\rangle$ corresponding to the values of magnetic field B_i and B_j is calculated.

B-VIII Schematic of additional system sizes.

TEE is calculated in additional system sizes $N = 7$ and $N = 13$ to verify the universality of the fluctuation in the helical phase. Figure B.10 shows the geometry of the respective spin system chosen. The Hamiltonian used is the same as the one used for the $N = 19$ case.

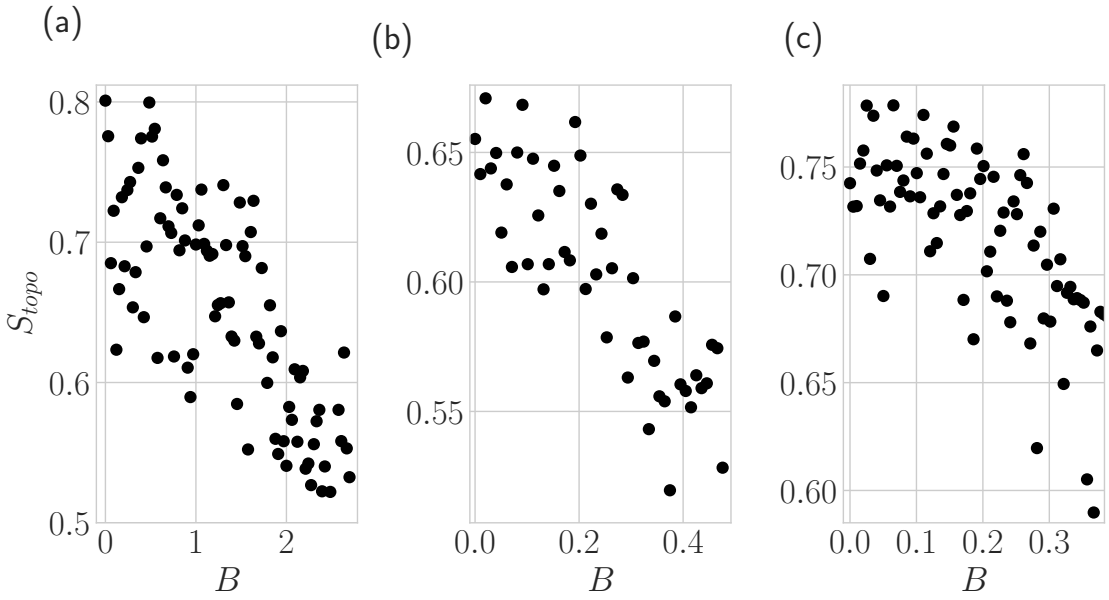

Fig. B.9 S_{topo} is calculated for (a) $N = 7$, (b) $N = 13$ and (c) $N = 19$.

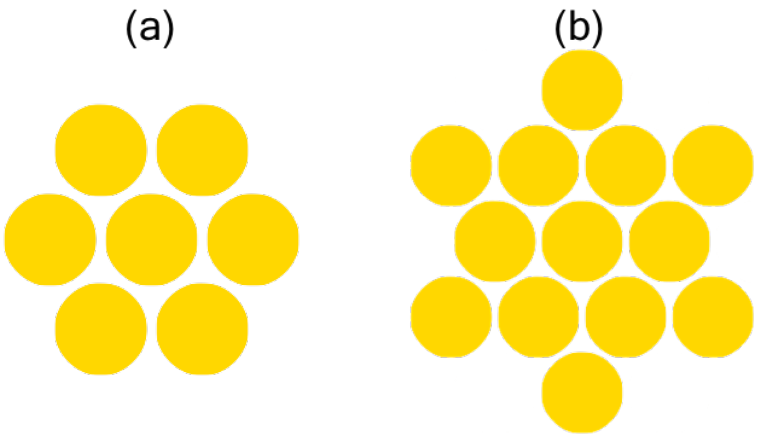

Fig. B.10 Schematic of the lattices considered a) N=7 and b) N=13.